8

The Newly Calculations of Production Cross Sections for Some Positron Emitting and Single Photon Emitting Radioisotopes in Proton Cyclotrons

E. Tel[1], M. Sahan[1], A. Aydin[2], H. Sahan[1], F. A.Ugur[1] and A. Kaplan[3]
[1] *Faculty of Arts and Science, Osmaniye Korkut Ata University,*
[2] *Faculty of Arts and Science, Kirikkale University*
[3]*Faculty of Arts and Science, Süleyman Demirel University*
Turkey

1. Introduction

Nowadays, radioisotopes are produced using both nuclear reactors and cyclotrons. Especially, the induced by intermediate and high energy protons nuclear reactions are very important because of a wide range technical applications. These reactions are required for advanced nuclear systems, such as spallation reaction for production of neutrons in spallation neutron source (capable of incinerating nuclear waste and producing energy), high energy proton induced fission for the radioisotope production alternatives etc. [1,2]. By using the intermediate proton induced reactions, we can directly produce radionuclides used in medicine and industry.

In the last decade, a big success has been provided on production and usage of the radionuclides. The radioisotopes obtained from using charged particles (proton, deuteron, alpha etc.) play an important role in medical applications [3-6]. A medical radioisotope can be classified as a diagnostic or a therapeutic radionuclide, depending on its decay properties. Radionuclides are used in diagnostic studies via emission tomography, i.e. Positron Emission Tomography (PET), Single Photon Emission Computed Tomography (SPECT), and Endoradiotheraphy (internal therapy with radio nuclides). In general, the diagnostic radioisotopes can also be classified into two groups; namely β^+–emitters (^{11}C, ^{13}N, ^{15}O, ^{18}F, ^{62}Cu, ^{68}Ga, etc.) and γ – emitters (^{67}Ga, ^{75}Se, ^{123}I, etc.). The use of positron emitting radioisotopes such as ^{11}C, ^{13}N, ^{15}O, and ^{18}F together with PET offers a highly selective and quantitative means for investigating regional tissue biochemistry, physiology and pharmacology [7]. The positron emitting nuclei which are neutron deficient isotopes are important for PET studies. Positrons annihilate with electrons emitting two photons ($E\gamma$=511 keV) in opposite direction. Most of the positron emitters are still being studied in terms of their applicability for diagnostic purposes. PET has been developing with the increasing number of clinical facilities raising interest in the use of PET in routine practice [8,9].

In the radioisotope production procedure, the nuclear reaction data are mainly needed for optimization of production rates. This process involves a selection of the projectile energy

range that will maximize the yield of the product cross section for nuclear reaction and minimize that of the radioactive impurities [5,6]. The total cross section of production yields are also important in accelerator technology from the point of view of radiation protection safety**.** The nuclear reaction calculations based on standard nuclear reaction models can be helpful for determining the accuracy of various parameters of nuclear models and experimental measurements. Today, experimental cross-sections are available in EXFOR file [7]. The theoretical calculations of production rates for different medical nucleus reactions were calculated in statistical equilibrium (compound) and pre-equilibrium model in literature [10-14].

In this study, the newly calculations of proton cyclotron production cross sections in some PET , SPECT and others used in medical applications radioisotopes used in medical applications were investigated in a range of 5–100 MeV incident proton energy range. Excitation functions for pre-equilibrium calculations were newly calculated by using hybrid model, geometry dependent hybrid (GDH) model. The reaction equilibrium component was calculated with a traditional compound nucleus model developed by Weisskopf-Ewing (W-E) model [16]. We have investigated the optimum energy range for proton cyclotron production cross sections. We have presented the decay data taken from the NUDAT database [23]. Calculated results were also compared with the available excitation functions measurements in EXFOR file [7]. The optimum energy range and the decay data for the investigated radionuclides are given in Table 1.

2. The nuclear reaction cross-section calculations

Calculations based on nuclear reaction models play an important role in the development of reaction cross sections [15]. For many years, it has been customary to divide nuclear reactions into two extreme categories. Firstly, there are very fast, direct reactions which on a time scale comparable to the time ($\cong 10^{-22}$ s) necessary for the projectile to traverse a nuclear diameter, involve simple nuclear excitations, and are non-statistical in nature. Secondly, there are equilibrium nucleus reactions which occur on a very much longer time scale ($\cong 10^{-16}$ to 10^{-18}s) where emissions can be treated by the nuclear statistical model. This second process can be described adequately with equilibrium nucleus theories developed by the Weisskopf-Ewing (W-E) [16] and Hauser-Feshbach [17]. Equilibrium nucleus wave function is very complicated, involving a large number of particle-hole excitations to which statistical considerations are applicable. The spectra of the emitted particles of equilibrium nucleus are approximately Maxwellian, and angular distributions of emitted particles are symmetric about 90 degrees. During the nineteen-fifties and sixties, evidence accumulated suggesting that in some nuclear reactions, it is not possible to understand all emission processes in terms of equilibrium nucleus and direct processes. This reaction is known as pre-equilibrium reaction. The pre-equilibrium reactions occur on time scale about 10^{-18} to 10^{-20} s. Deviations from a Maxwellian shape for the emission spectra were observed for intermediate to high emission energies, with the theory under predicting data. The first developments were made to understand these observations by Griffin [18], who proposed the pre-equilibrium 'exciton model'. Pre-equilibrium processes are important mechanisms in nuclear reactions induced by light projectiles with incident energies above about 8-10 MeV. After Griffin introduced the exciton model, a series of semi-classical models [19-21] of varying complexities have been developed for calculating and evaluating particle emissions in the continuum. More recently, researchers have formulated several quantum–mechanical reaction theories [22] that are based on multi-step concepts and in which

statistical evaporation at lower energies is connected to direct reactions at higher energies. The hybrid model for pre-compound decay is formulated by Blann [19] as

$$\frac{d\sigma_{\upsilon}(\varepsilon)}{d\varepsilon} = \sigma_R P_{\upsilon}(\varepsilon)$$

$$P_{\upsilon}(\varepsilon)d\varepsilon = \sum_{\substack{n=n_0 \\ \Delta n=+2}}^{\bar{n}} \left[{}_n\chi_{\upsilon} N_n(\varepsilon,U) / N_n(E) \right] g\, d\varepsilon \left[\lambda_c(\varepsilon) / (\lambda_c(\varepsilon) + \lambda_+(\varepsilon)) \right] D_n \quad (1)$$

where $P_{\upsilon}(\varepsilon)d\varepsilon$ represents number of particles of the ν type (neutron or proton) emitted into the unbound continuum with channel energy between ε and $\varepsilon + d\varepsilon$. The quantity in the first set of square brackets of Eq.(1) represents the number of particles to be found (per MeV) at a given energy (with respect to the continuum) for all scattering processes leading to an "n" exciton configuration. It has been demonstrated that the nucleon-nucleon scattering energy partition function Nn(E) is identical to the exciton state density ρn(E). The second set of square brackets in Eq. (1) represents the fraction of the ν type particles at energy, which should undergo emission into the continuum, rather than making an intra-nuclear transition. The Dn represents the average fraction of the initial population surviving to the exciton number being treated. Early, $\lambda_c(\varepsilon)$ is emission rate of a particle into the continuum with channel energy ε and $\lambda_+(\varepsilon)$ is the intranuclear transition rate of a particle. Nn (ε ,U) is the number of ways. comparisons between experimental results, pre-compound exciton model calculations, and intra-nuclear cascade calculations indicated that the exciton model gave too few pre-compound particles and that these were too soft in spectral distribution for the expected initial exciton configurations. The intra-nuclear cascade calculation results indicated that the exciton model deficiency resulted from a failure to properly reproduce enhanced emission from the nuclear surface. In order to provide a first order correction for this deficiency the hybrid model was reformulated by Blann and Vonach [24]. In this way the diffuse surface properties sampled by the higher impact parameters were crudely incorporated into the pre-compound decay formalism, in the geometry dependent hybrid (GDH) model. The differential emission spectrum is given in the GDH model as

$$\frac{d\sigma_{\upsilon}(\varepsilon)}{d\varepsilon} = \pi \lambda\!\!\!^{-2} \sum_{l=0}^{\infty} (2l+1) T_l P_{\upsilon}(l,\varepsilon) \quad (2)$$

where $\lambda\!\!\!^{-}$ is reduced de Broglie wavelength of the projectile and T_l represents transmission coefficient for *l* th partial wave ℓ is orbital angular momentum in *n* unit $\hbar$.

3. Results and discussion

This work describes new calculations on the excitation functions of $^{18}O(p,n)^{18}F$, $^{57}Fe(p,n)^{57}Co$, $^{57}Fe(p,\alpha)^{54}Mn$, $^{68}Zn(p,2n)^{67}Ga$, $^{68}Zn(p,n)^{68}Ga$, $^{93}Nb(p,4n)^{90}Mo$, $^{112}Cd(p,2n)^{111}In$, $^{127}I(p,3n)^{125}Xe$,$^{133}I(p,6n)^{128}Ba$ and $^{203}Tl(p,3n)^{201}Pb$ reactions carried out in the 5-100 MeV proton energy range. The pre-equilibrium calculations involve the hybrid model and the geometry dependent hybrid (GDH) model. Equilibrium reactions have been calculated according to Weisskopf–Ewing (W-E) model. The ALICE/ASH code was used in the calculations of all models described above. The ALICE/ASH code is an advanced and modified version of the ALICE

codes. The modifications concern the implementation in the code of models describing the pre-compound composite particle emission, fast γ-emission, different approaches for the nuclear level density calculation, and the model for the fission fragment yield calculation. The ALICE/ASH code can be applied for the calculation of excitation functions, energy and angular distribution of secondary particles in nuclear reactions induced by nucleons and nuclei with the energy up to 300 MeV. The initial exciton number as n_o =3 and the exciton numbers (for protons and neutrons) in the calculations for proton induced reactions as,

$$ {}_3X_p = 2\frac{\left(\sigma_{pn}/\sigma_{pp}\right)N + 2Z}{2(\sigma_{pn}/\sigma_{pp})N + 2Z}, \quad {}_3X_n = 2 - {}_3X_p \tag{3} $$

where σ_{xy} is the nucleon-nucleon interaction cross-section in the nucleus. Z and N are the proton and neutron numbers, respectively, of the target nuclei. The ratio of nucleon-nucleon cross-sections calculated taking into account to Pauli principle and the nucleon motion is parameterized

$$ \sigma_{pn}/\sigma_{pp} = \sigma_{np}/\sigma_{nn} = 1.375\times10^{-5}T^2 - 8.734\times10^{-3}T + 2.776 \tag{4} $$

where T is the kinetic energy of the projectile outside the nucleus. The super-fluid model [26] has been applied for nuclear level density calculations in the ALICE/ASH code. The results of the calculations are plotted in [Fig. 1], [Fig. 2], [Fig. 3], [Fig. 4], [Fig. 5], [Fig. 6], [Fig. 7], [Fig. 8], [Fig. 9], and [Fig. 10]. Calculated results based on hybrid model, geometry dependent hybrid model and equilibrium model have been compared with the experimental data. The experimental taken from EXFOR [7] are shown with different symbols (such as +, o, Δ) symbols in all figures. The results are given below.

3.1 $^{18}O(p,n)^{18}F$ reaction process

The calculation for the excitation function of $^{18}O(p,n)^{18}F$ reaction has been compared with the experimental values in Fig.1. In general, the hybrid model calculations are the best agreement with the measurements of $^{18}O(p,n)^{18}F$ reaction up to 30 MeV the incident proton energy. The equilibrium W-E model calculations are only in agreement with in energy region lower than 20 MeV. The optimum energy range for production of ^{18}F is E_p= 10 → 5 MeV.

3.2 $^{57}Fe(p,n)^{57}Co$ reaction process

The calculation cross section of $^{57}Fe(p,n)^{57}Co$ reaction has been compared with the experimental values in Fig.2. The hybrid model calculations are the best agreement with the measurements of Levkovskij [7] at above the 20 MeV energie regions. The W-E model calculations are only in agreement with in energy region lower than 20 MeV. The GDH model calculations are a little higher than the measurements of Levkovskij [7] at above the 20 MeV for incident proton energies. The optimum energy range for production of ^{57}Co is E_p= 15 → 5 MeV.

3.3 $^{57}Fe(p,\alpha)^{54}Mn$ reaction process

The calculated $^{57}Fe(p,\alpha)^{54}Mn$ reaction has been compared with the experimental values in Fig.3. The hybrid model and GDH model calculations are in good agreement with the measurements of Levkovskij [7] at above the 20 MeV energie regions. The W-E model calculations are good in agreement with in energy region lower than 20 MeV. The optimum energy range for production of ^{54}Mn is E_p= 20 → 10 MeV.

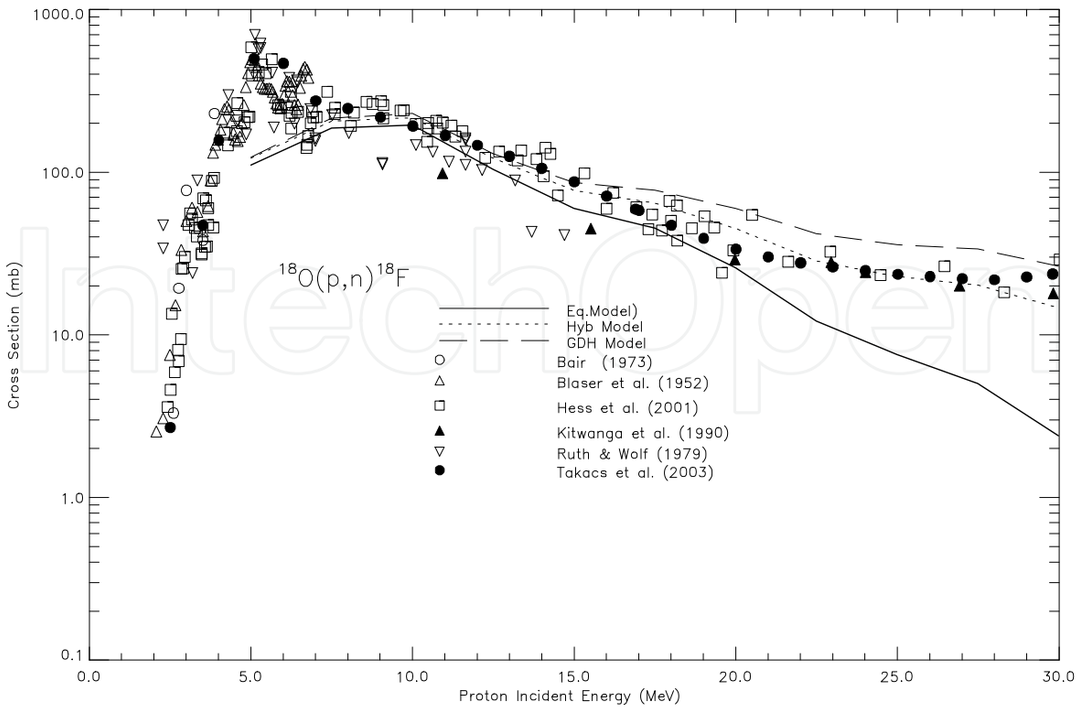

Fig. 1. The comparison of the calculated cross section of $^{18}O(p,n)^{18}F$ reaction with the values reported in Ref. [7].

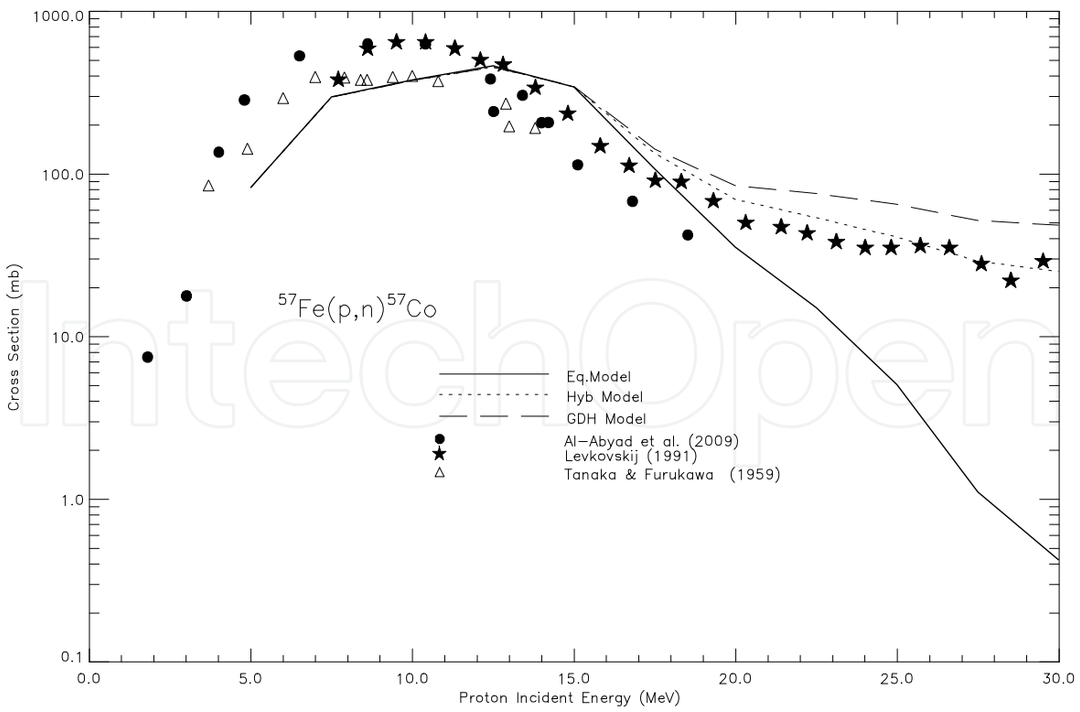

Fig. 2. The comparison of the calculated cross section of $^{57}Fe(p,n)^{57}Co$ reaction with the values reported in Ref. [7].

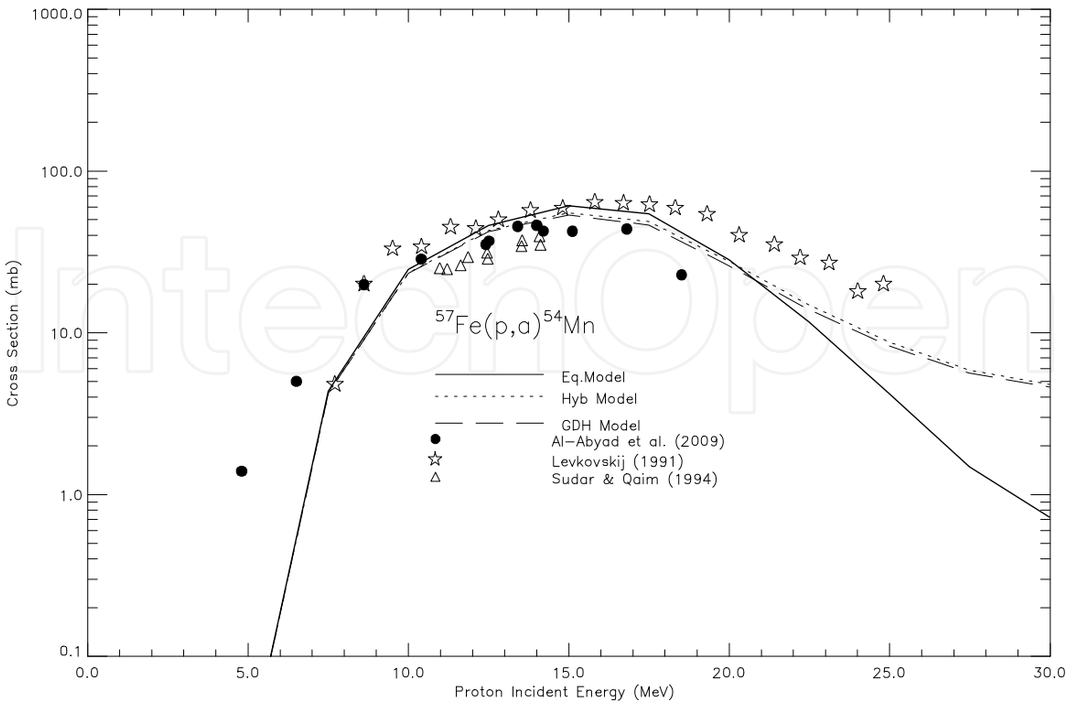

Fig. 3. The comparison of the calculated cross section of $^{57}Fe(p,\alpha)^{54}Mn$ reaction with the values reported in Ref. [7].

3.4 $^{68}Zn(p,2n)^{67}Ga$ reaction process

The calculation on the excitation function of $^{68}Zn(p,n)^{67}Ga$ reaction has been compared with the experimental values in Fig.4. The W-E model calculations are in agreement with the measurements up to 25 MeV. Also, the GDH and hybrid model calculations are in very good harmony with the experimental data. The optimum energy range for production of ^{67}Ga is E_p= 30 →15 MeV.

3.5 $^{68}Zn(p,n)^{68}Ga$ reaction process

The calculation on the excitation function of $^{68}Zn(p,n)^{68}Ga$ reaction has been compared with the experimental values in Fig.5. The experimental data of the measurements are in good agreement with each other. The W-E model calculations are in agreement with the measurements up to 15 MeV. The GDH model calculations are the best agreement with the experimental data of 5 – 30 MeV energy range. Also, the hybrid model calculations are in very good harmony with the experimental data. The optimum energy range for production of ^{68}Ga is E_p= 15 → 5 MeV.

3.6 $^{93}Nb(p,4n)^{90}$ Mo reaction process

The calculation on the excitation function of $^{93}Nb(p,4n)^{90}Mo$ reaction has been compared with the experimental values of Ditroi *et al.* [7] in Fig.6. While the GDH model calculations are the best agreement with the experimental data of 35 – 60 MeV energy range, the other model calculations are higher than the experimental data. The optimum energy range for production of ^{90}Mo is E_p= 55 →45 MeV.

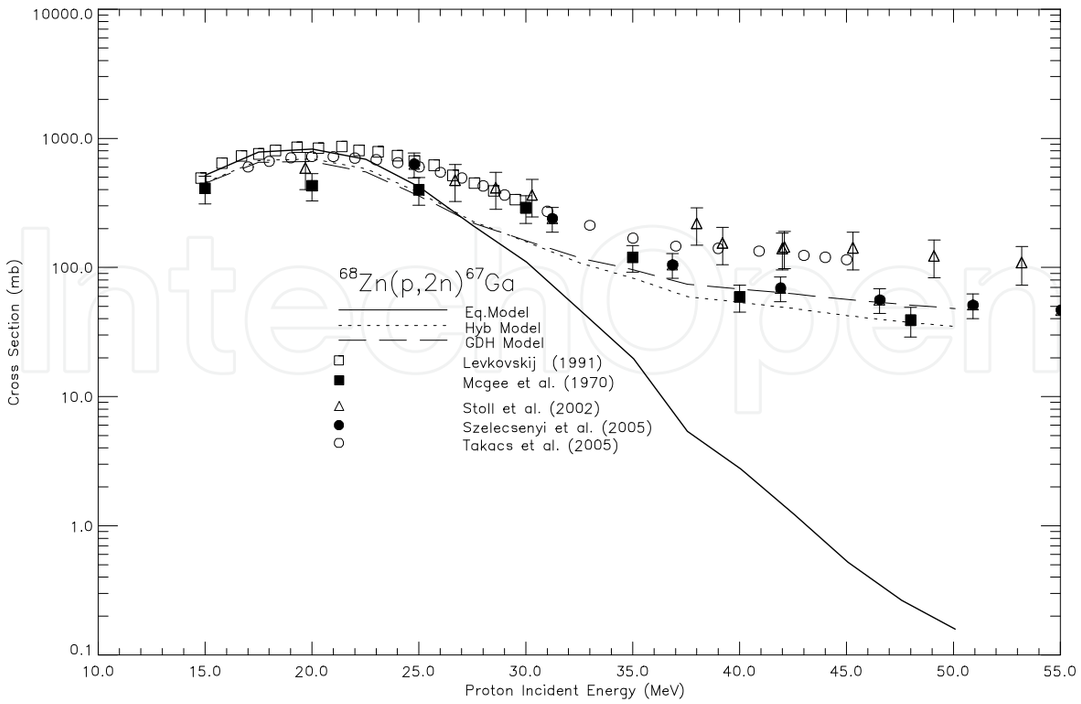

Fig. 4. The comparison of the calculated cross section of ^{68}Zn(p,2n)^{67}Ga reaction with the values reported in Ref. [7].

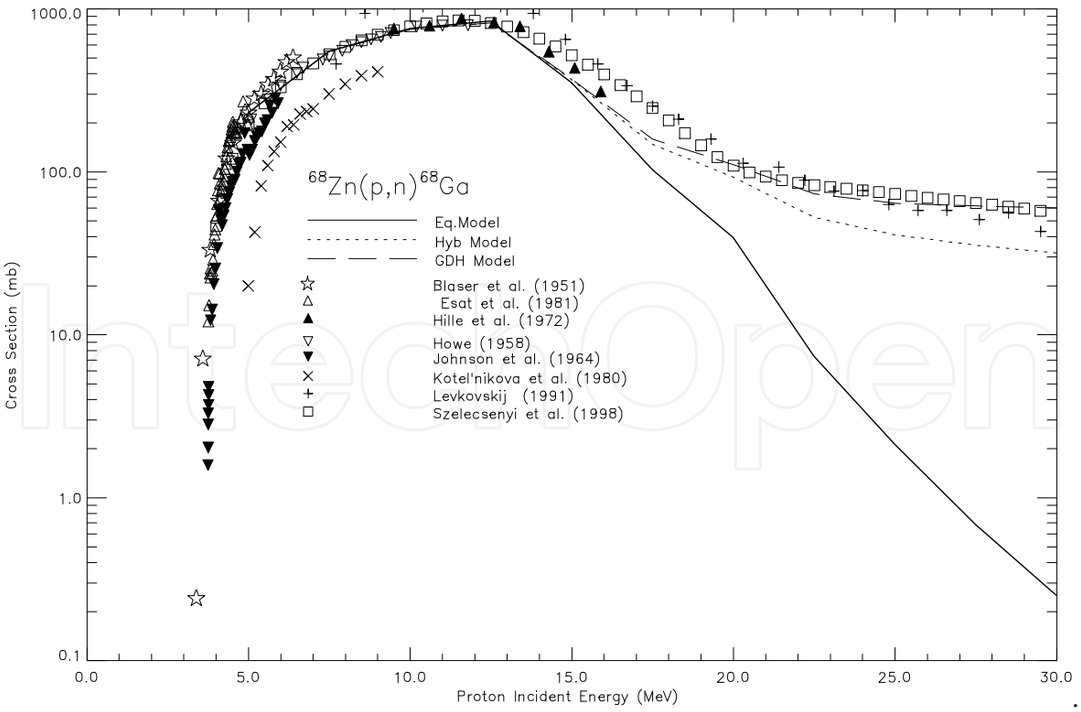

Fig. 5. The comparison of the calculated cross section of ^{68}Zn(p,n)^{68}Ga reaction with the values reported in Ref. [7].

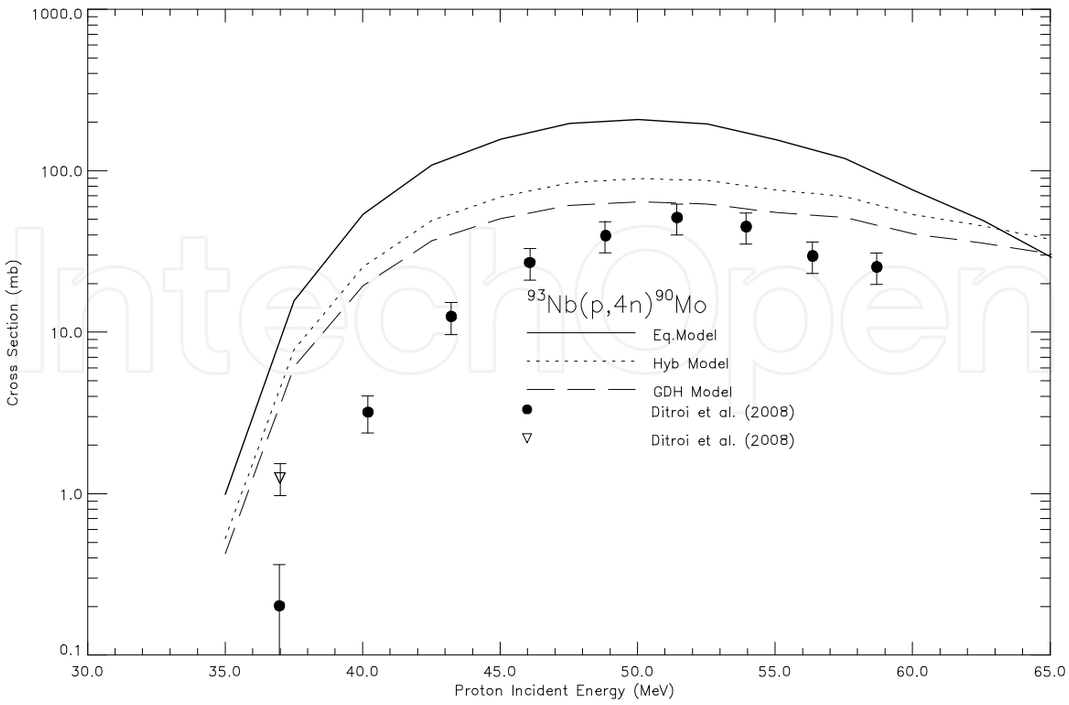

Fig. 6. The comparison of the calculated cross section of ^{93}Nb(p,4n)^{90}Mo reaction with the values reported in Ref. [7].

3.7 ^{112}Cd(p,2n)^{111}In reaction process

Especially, the ^{111}In radionuclei are very important for SPECT. The calculation on the excitation function of ^{112}Cd(p,2n)^{111}In reaction has been compared with the experimental values in Fig.7. Generally, the experimental data of the measurements are in good agreement with each other. The GDH and hybrid model calculations are in very good harmony with the experimental data. The equilibrium W-E model calculations are in agreement with the measurements up to 30 MeV. The optimum energy range for production of ^{111}In is E_p= 25 →15 MeV.

3.8 ^{127}I(p,3n)^{125}Xe reaction process

The calculation on the excitation function of ^{127}I(p,3n)^{125}Xe reaction has been compared with the experimental values in Fig.8. We can say that the experimental data of the measurements are in good agreement with each other. The equilibrium W-E model calculations are in agreement with experimental values up to 35 MeV The GDH and hybrid model calculations are in very good harmony with the experimental data. The optimum energy range for production of ^{125}Xe is E_p= 35 →25 MeV.

3.9 ^{133}Cs(p,6n)^{128}Ba reaction process

The calculation on the excitation function of ^{133}Cs(p,6n)^{128}Ba reaction has been compared with the experimental values in Fig.9. The equilibrium W-E model calculations are not agreement with experimental values. The GDH model calculations are the best agreement with the experimental data of Deptula *et al.* [7] for 45-100 MeV energy range. While the hybrid model calculations are the good agreement with the experimental data of 45-65 MeV energy range, for above the 65 MeV proton incident energy this model calculations are higher than the experimental data.The optimum energy range for production of ^{128}Ba is E_p= 70 →50 MeV.

3.10 ^{203}Tl(p,3n)^{201}Pb reaction process

The ^{201}Tl radioisotopes are very important for using in the SPECT. The reaction process for ^{201}Tl is ^{203}Tl(p,3n)^{201}Pb, $^{201}Pb \xrightarrow{9.33h} {}^{201}Tl$. The calculation on the excitation function of ^{203}Tl(p,3n)^{201}Pb reaction has been compared with the experimental values of Blue *et al* [7], Lebowitz *et al.* [7] and Al-saleh *et al.* [7] Takacs *et al.* [7] in Fig.8. The Weisskopf-Ewing model calculations are in agreement with the measurements up to 35 MeV. The GDH model and hybrid model calculations are in good agreement with the experimental data of 20 – 35 MeV energy range. The optimum energy range for production of ^{201}Tl is E_p= 30→ 20 MeV.

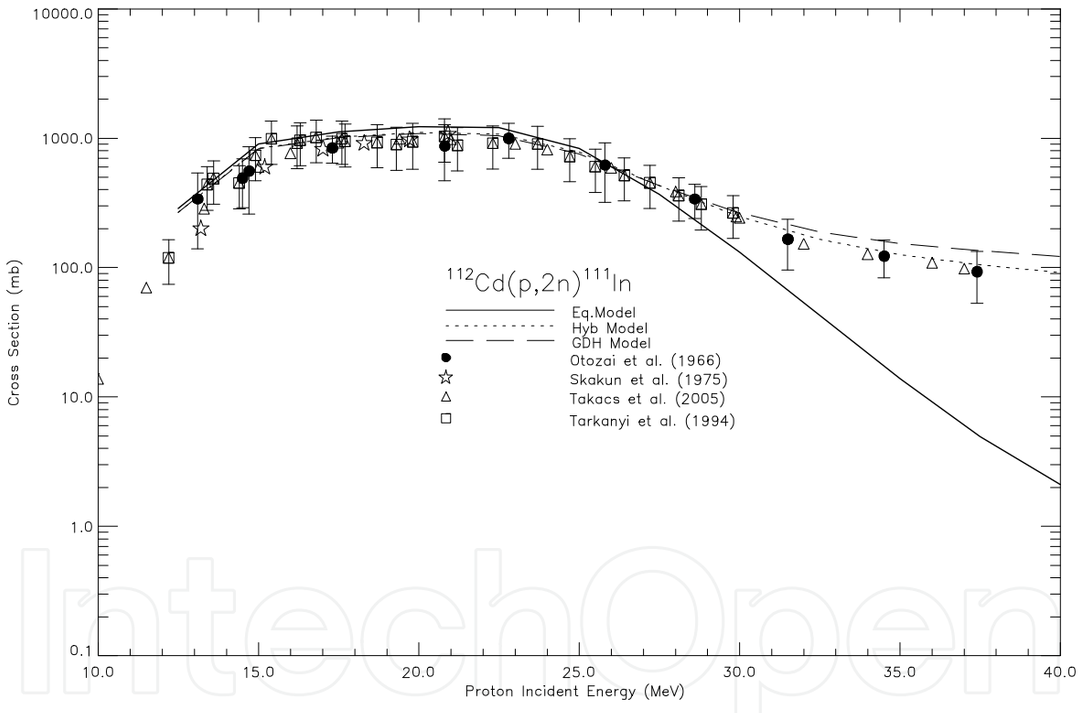

Fig. 7. The comparison of the calculated cross section of ^{112}Cd(p,2n)^{111}In reaction with the values reported in Ref. [7].

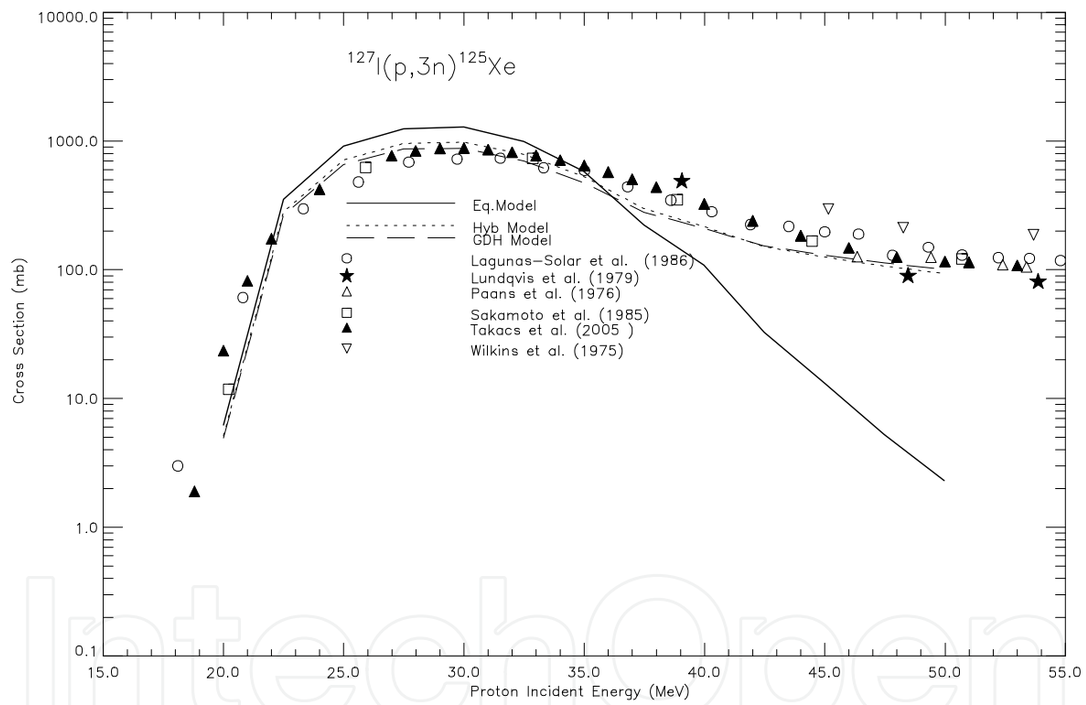

Fig. 8. The comparison of the calculated cross section of $^{127}I(p,3n)^{125}Xe$ reaction with the values reported in Ref. [7].

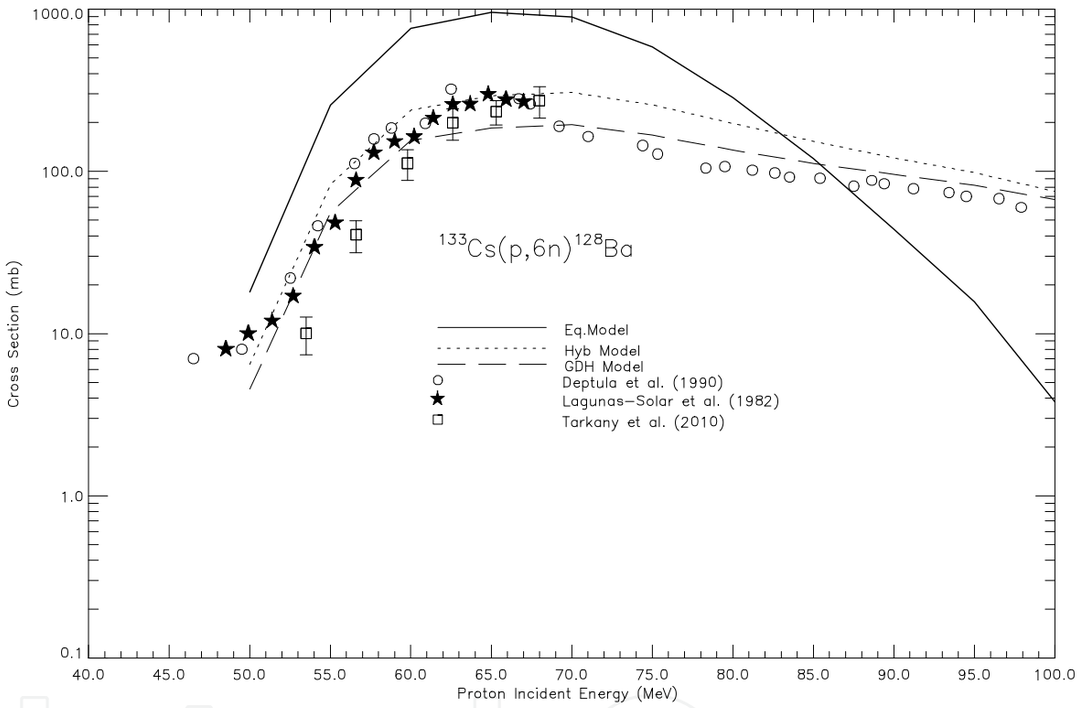

Fig. 9. The comparison of the calculated cross section of $^{133}Cs(p,6n)^{128}Ba$ reaction with the values reported in Ref. [7].

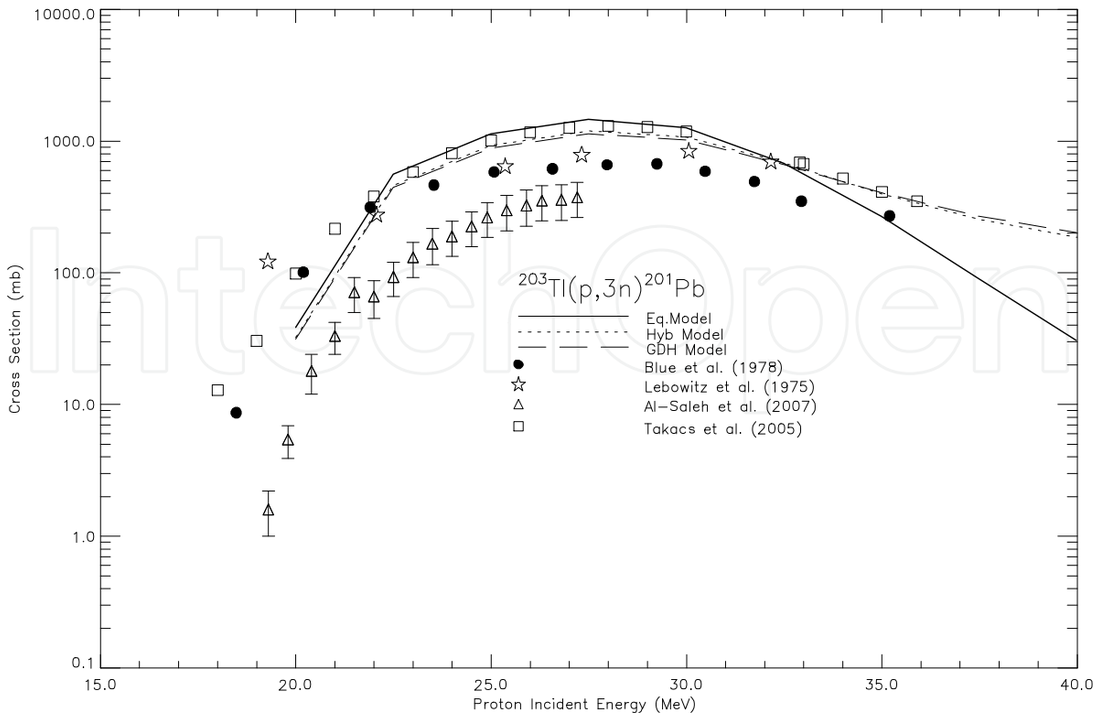

Fig. 10. The comparison of the calculated cross section of ^{203}Tl(p,3n)^{201}Pb reaction with the values reported in Ref. [7].

Producted radioisotopes	Half life	Mode of decay (%)	$E_{\square}$ (keV)	$I_{\square\square}$(%)	Optimum Energy Range (MeV)
^{18}F	1.83 h	EC + β^+ (100)	0.52	0.01795	E_p= 10 → 5
^{57}Co	271.74 d	EC + β^+ (100)	122.06065	85.60	E_p= 15 → 5
^{54}Mn	312.05d	EC + β^+ (100)	834.848	99.97	E_p= 20 → 10
^{67}Ga	3.2617 d	EC + β^+ (100)	393.527	4.56	E_p= 30 →15
^{68}Ga	67.63m	EC+ β^+ (100)	1077.35	3	E_p= 15 → 5
^{90}Mo	5.67h	EC + β^+ (100)	257.34	78	E_p= 55 →45
^{111}In	2.8047 d	EC + β^+ (100)	245.350	94.10	E_p= 25 →15
^{125}Xe	56.9s	EC + β^+ (100)	111.3	60.2	E_p= 35 →25
^{128}Ba	2.43d	EC + β^+ (100)	273.44	14.5	E_p= 70 →50
^{201}Pb	9.33 h	EC+ β^+ (100)	546.280	0.279	E_p= 30→ 20

Table 1. The decay data and optimum energy range for investigated radionuclides.

4. Conclusions

The new calculations on the excitation functions of $^{18}O(p,n)^{18}F$, $^{57}Fe(p,n)^{57}Co$, $^{57}Fe(p,\alpha)^{54}Mn$, $^{68}Zn(p,2n)^{67}Ga$, $^{68}Zn(p,n)^{68}Ga$, $^{93}Nb(p,4n)^{90}Mo$, $^{112}Cd(p,2n)^{111}In$, $^{127}I(p,3n)^{125}Xe$,$^{133}I(p,6n)^{128}Ba$ and $^{203}Tl(p,3n)^{201}Pb$ reactions have been carried out using nuclear reaction models. Although there are some discrepancies between the calculations and the experimental data, in generally, the new evaluated hybrid and GDH model calculations (with ALICE/ASH) are good agreement with the experimental data above the incident proton energy with 5-100 MeV in Figs. 1-10. While the Weisskopf-Ewing model calculations are only in agreement with the measurements for lower incident proton energy regions, hybrid model calculations are in good harmony with the experimental data for higher incident proton energy regions. Some nuclei used in this study were examined and compared in previous paper written by Tel et al.[13,14]. Detailed informations can be found in these papers. And also new developed semi-empirical formulas for proton incident reaction cross-sections can be found in Ref. [27,28].

When Comparing the experimental data and theoretical calculations, the production of ^{18}F,^{57}Co, ^{54}Mn, $^{67,68}Ga$, ^{90}Mo, ^{111}In, ^{125}Xe , ^{128}Ba and ^{201}Pb radioisotopes can be employed at a medium-sized proton cyclotron since the optimum energy ranges are smaller than 50 MeV, except for ^{128}Ba. We gave the optimum energy range and the decay data for the investigated radionuclides in Table 1.

5. References

[1] M B Chadwick, P G Young, S Chiba, S C Frankle, G M Hale, H G Hughes, A J Koning, R C Little, R E MacFarlane, R E Prael, L S Waters, *Nucl. Sci. Engin*. 131 293 (1999)

[2] C. Rubbia, J A Rubio, S Buorno, F Carminati, N Fitier, J Galvez, C Gels, Y Kadi, R Klapisch, P Mandrillon, J P Revol, and Ch. Roche, *European Organization for Nuclear Research,* CERN/AT/95-44 (ET) (1995).

[3] S M Qaim *Radiat. Phys. Chem.* 71 917 (2004).

[4] S M Qaim *Radiochim. Acta* 89 297 (2001).

[5] B Scholten, E Hess, S Takacs, Z Kovacs, F Tarkanyi, H H Coenen and S M Qaim *J. Nucl. Sci. and Tech.* 2 1278 (2002).

[6] S M Qaim Radiochim. *Acta* 89 223 (2001).

[7] EXFOR/CSISRS (Experimental Nuclear Reaction Data File), Brookhaven National Laboratory, National Nuclear Data Center, (http://www.nndc.bnl.gov/exfor/) (2009) .

[8] A P Wolf, J S Fowler *Positron Emitter Labeled Radiotracers, Chemical Considerations in Positron Emission Tomography* (Alan R. Liss, Inc. Pub.) (1985) .

[9] A P Wolf and W B Jones *Radiochim. Acta* 34 1 (1983).

[10] K Gul *Appl. Radiat. Isotopes* 54 147 (2001).

[11] K Gul *Appl. Radiat. Isotopes* 54 311 (2001).

[12] A Aydın, B Sarer, E Tel *Appl. Radiat. Isotopes* 65 365 (2007).

[13] E Tel, E G Aydin, A. Kaplan and A. Aydin, *Indian J. Phys.* 83 (2) 1-20 (2009).

[14] E G Aydin, E Tel, A Kaplan and A Aydin, *Kerntechnic,* 73, 4, (2008).

[15] M B Chadwick *Radiochim. Acta* 89 325 (2001).

[16] V F Weisskopf and D H Ewing *Phys. Rev*. 57 472 (1940) .

[17] W Hauser and H Feshbach *Phys. Rev*. 87 366 (1952) .

[18] J J Griffin, *Phys. Rev. Lett*. 17 478 (1966) .

[19] M Blann *Annu. Rev. Nucl. Sci.* 25 123 (1975) .
[20] E Betak *Comp. Phys. Com.* 9 92 (1975).
[21] H. Gruppelaar, P Nagel, P E Hodgson and LaRivasta Del *Nuovo Cim.* 9 1 (1986).
[22] H Feshbach, A Kerman and S Koonin *Annu.Phys.* (NY), 125 429 (1980) .
[23] NUDAT – Decay Radiation Database, http://www.nndc.bnl.gov/nudat2
[24] M Blann and H K Vonach *Phys. Rev.* C28 1475 (1983).
[25] C. H. M. Broeders, A. Yu. Konobeyev, Yu. A. Korovin, et al., http://bibliothek.fzk.de/zb/berichte/FZKA7183.pdf.
[26] A. V. Ignatyuk, K. K. Istekov, G. N. Smirenkin, *Yad. Fiz.* 29, 875 (1979).
[27] Tel, E., Aydın, E. G., Aydın, A., Kaplan, A., *Appl. Radiat. Isotopes* 67 (2), 272 (2009)
[28] Tel, E., Aydın, A., Aydın, E. G., Kaplan, A., Ö. Yavaş, İ. Reyhancan, , *Pramana-J. Phys.,* 74 (6), 931-944, (2010).

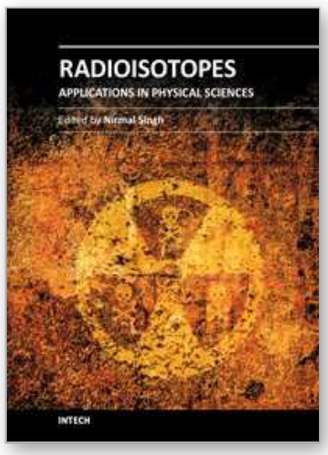

Radioisotopes - Applications in Physical Sciences

Edited by Prof. Nirmal Singh

ISBN 978-953-307-510-5
Hard cover, 496 pages
Publisher InTech
Published online 19, October, 2011
Published in print edition October, 2011

The book Radioisotopes - Applications in Physical Sciences is divided into three sections namely: Radioisotopes and Some Physical Aspects, Radioisotopes in Environment and Radioisotopes in Power System Space Applications. Section I contains nine chapters on radioisotopes and production and their various applications in some physical and chemical processes. In Section II, ten chapters on the applications of radioisotopes in environment have been added. The interesting articles related to soil, water, environmental dosimetry/tracer and composition analyzer etc. are worth reading. Section III has three chapters on the use of radioisotopes in power systems which generate electrical power by converting heat released from the nuclear decay of radioactive isotopes. The system has to be flown in space for space exploration and radioisotopes can be a good alternative for heat-to-electrical energy conversion. The reader will very much benefit from the chapters presented in this section.

How to reference

In order to correctly reference this scholarly work, feel free to copy and paste the following:

E. Tel, M. Sahan, A. Aydin, H. Sahan, F. A.Ugur and A. Kaplan (2011). The Newly Calculations of Production Cross Sections for Some Positron Emitting and Single Photon Emitting Radioisotopes in Proton Cyclotrons, Radioisotopes - Applications in Physical Sciences, Prof. Nirmal Singh (Ed.), ISBN: 978-953-307-510-5, InTech, Available from: http://www.intechopen.com/books/radioisotopes-applications-in-physical-sciences/the-newly-calculations-of-production-cross-sections-for-some-positron-emitting-and-single-photon-emi

INTECH
open science | open minds

InTech Europe
University Campus STeP Ri
Slavka Krautzeka 83/A
51000 Rijeka, Croatia
Phone: +385 (51) 770 447
Fax: +385 (51) 686 166
www.intechopen.com

InTech China
Unit 405, Office Block, Hotel Equatorial Shanghai
No.65, Yan An Road (West), Shanghai, 200040, China
中国上海市延安西路65号上海国际贵都大饭店办公楼405单元
Phone: +86-21-62489820
Fax: +86-21-62489821

IntechOpen